

Article

Multipurpose Quantum Simulator Based on a Hybrid Solid-State Quantum Device

Tingting Yuan ¹, Fang Zhou ^{1,2,3} , Shengping Chen ⁴, Shaohua Xiang ¹, Kehui Song ¹ and Yujing Zhao ^{1,*} 

¹ College of Mechanical Engineering and Photoelectric Physics, Hunan Engineering Laboratory for Preparation Technology of Polyvinyl Alcohol Fiber Material, Huaihua University, Huaihua 418008, China; chuiwennalan@163.com (T.Y.); zhoufang@hhct.edu.cn (F.Z.); shxiang97@163.com (S.X.); hkhsong@vip.sina.com (K.S.)

² Department of Basic Course, Hunan Police Academy, Changsha 410138, China

³ Synergetic Innovation Center for Quantum Effects and Application, Key Laboratory of Low-Dimensional Quantum Structures and Quantum Control of Ministry of Education, School of Physics and Electronics, Hunan Normal University, Changsha 410081, China

⁴ School of Software, Jishou University, Zhangjiajie 427000, China; shengpingchen@jsu.edu.cn

* Correspondence: zhaoyujing@hhct.edu.cn; Tel.: +86-0745-2851011

Received: 11 February 2019; Accepted: 26 March 2019; Published: 2 April 2019



Abstract: This paper proposes a scheme to enhance the fidelity of symmetric and asymmetric quantum cloning using a hybrid system based on nitrogen-vacancy (N-V) centers. By setting different initial states, the present scheme can implement optimal symmetric (asymmetric) universal (phase-covariant) quantum cloning, so that the copies with the assistance of a Current-biased Josephson junction (CBJJ) qubit and four transmission-line resonators (TLRs) can be obtained. The scheme consists of two stages: the first stage is the implementation of the conventional controlled-phase gate, and the second is the realization of different quantum cloning machines (QCM) by choosing a suitable evolution time. The results show that the probability of success for QCM of a copy of the equatorial state can reach 1. Furthermore, the $|W_4^\pm\rangle$ entangled state can be generated in the process of the phase-covariant quantum anti-cloning. Finally, the decoherence effects caused by the N-V center qubits and CBJJ qubit are discussed.

Keywords: multipurpose quantum simulator; hybrid solid-state quantum device; $|W_4^\pm\rangle$ entangled state; N-V center

1. Introduction

It is well-known that an unknown quantum state cannot be copied precisely [1]. The original paper of this theorem [1] shows that the quantum no-cloning theorem is a consequence of the quantum state superposition principle. Despite strict restriction, several similar QCMs are proposed. For example, for an unknown quantum state, we can either obtain the imperfect copies [2] or perfect copies with non-zero probability of failure [3].

In recent years, much effort has been made to study QCM theoretically and experimentally, including the universal QCM [4–7], probabilistic quantum cloning [3,8], state-dependent cloning [9], phase-covariant quantum cloning [10–12], quantum cloning in separate cavities via the optical coherent pulse as a quantum communication bus [13], economical state-dependent telecloning [14,15], and quantum jointly assisted cloning [16].

Quantum cloning is mainly applied in two fields. One is wiretap in quantum cryptography, and the other is quantum computation. Application of wiretap in quantum cryptography is based mostly on approximate quantum cloning [17,18]. In the application process, incomplete replication

is permissible. As is commonly known, phase-covariant QCM could optimally clone the state in a Bloch ball equator in the form of $|\psi\rangle = \frac{1}{\sqrt{2}}(|0\rangle + e^{i\phi}|1\rangle)$. Phase-covariant QCM plays an important role in applications in quantum cryptography, and it has a higher quality of reproduction of all equator states than common QCM. This could be realized by coupling the system to be cloned to the auxiliary system. To work out the operating scheme which could realize quantum cloning easily, it is necessary to find out an appropriate quantum system, which should be easy to operate with good environmental isolation so that the influences of de-coherence can be effectively avoided.

The new system connected four N-V centers and four TLRs by CBJJ. The N-V center(1) carries the quantum state to be cloned, while the N-V center(2,3) are the clone quantum bits. The CBJJ is the auxiliary quantum bit. The four TLRs are the data bus, and are connected to one another through the CBJJ. Besides the special functions of different QCM, this system could also realize phase-covariant quantum anti-cloning and generate the $|W_4^\pm\rangle$ entangled state. Based on this, the new scheme, which could realize the multi-purpose quantum simulator of the equator state with a high retainment of quantum cloning, is put forward. Compared with various related studies we have investigated and examined [8,12,14–16], this scheme has obvious advantages. Firstly, interactions between CBJJ (NV) and TLRs could easily control the quantum cloning process by adjusting the external parameters of the CBJJ and the frequencies of all the TLRs. Secondly, in the quantum cloning scheme put forward in the study, only a controlled-NOT gate operation is required, and there are three quantum bits in the final state of ancilla. The operation process of the scheme is simple, with less auxiliary quantum bits, which could guarantee the high quality of the system's reproduction. Thirdly, in the process of quantum anti-cloning, it requires only Equation (9) to complete the quantum anti-cloning, in which the CBJJ functions as the catalyst—in other words, its state is always retained in the ground state $|g\rangle$. Thus, a noticeable feature of the anti-cloning scheme is that the TLRs only remain in the virtual excited state, which means that the de-coherence caused by TLRs could be neglected. Besides, the $|W_4^\pm\rangle$ entangled state could be prepared in the process of quantum anti-cloning. Finally, after the conversion of quantum cloning is completed, the initial quantum state could be pre-processed, which could make the duplicates obtained have a high quality of reproduction. Therefore, effective use of quantum resources could make our scheme an economical one. This is feasible in quantum information processing. The remainder of this essay is as follows: Section 3 introduces three interactive Hamiltonian functions of the system; Section 4 introduces our scheme in detail, which could be used to realize a multi-purpose quantum simulator and be used for equator state quantum cloning, with a high quality of reproduction; Section 5 discusses how to realize quantum anti-cloning, and to generate the $|W_4^\pm\rangle$ entangled state. Finally, a conclusion is made in Section 6.

2. Basic Theory

There are three interacting Hamiltonians in the system.

2.1. CBJJ–TLR Off-Resonant Interaction

As shown in Figure 1a, the Hamiltonian of the j th TLR is ($\hbar = 1$) [19]

$$H_T^j = \omega_c^j a_j^\dagger a_j, \quad (1)$$

where a_j , (a_j^\dagger) is the annihilation (creation) operator, $\omega_c^j = 2\pi / (\sqrt{F_t^j C_t^j})$ is the frequency of the j th TLR, and F_t^j and C_t^j is the inductance and capacitance of the j th TLR, respectively.

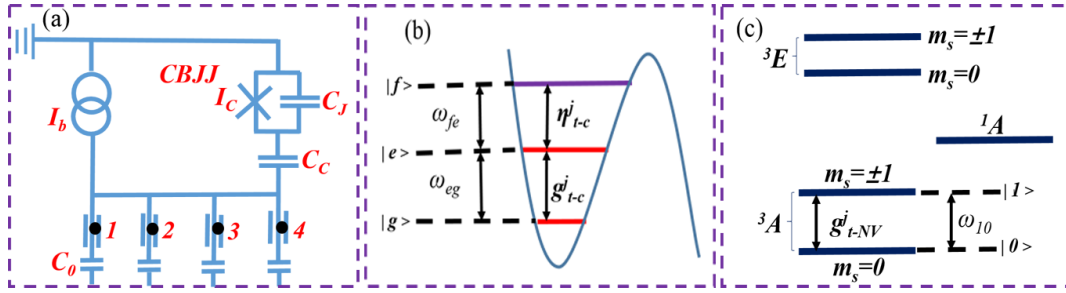


Figure 1. (a) Diagram of a CBJJ coupled to four TLRs via the coupling capacitor, C_c . The black dot in each TLR represents a N-V center. (b) Level diagram for the CBJJ. The CBJJ is modelled as a particle with three levels: $|g\rangle$, $|e\rangle$, and $|f\rangle$, and ω_{fe} (ω_{eg}) is the transition frequency between the levels $|e\rangle$ and $|f\rangle$ ($|g\rangle$ and $|e\rangle$). (c) Level diagram for the j th N-V center, where ω_{10} is the transition frequency between the lowest level $m_s = 0$ and the degenerated level $m_s = \pm 1$.

As shown in Figure 1b, the energy level $|g\rangle$ is the energy zero-point, and the frequency $\omega_{eg} \simeq 0.9\omega_p$, $\omega_{fe} \simeq 0.81\omega_p$ is the plasma oscillation frequency, where $\omega_p = (2\pi I_c / \Phi_0 C_J)^{1/2} [1 - (I_b / I_c)^2]^{1/4}$ is the plasma oscillation frequency [20], with $\Phi_0 = 1/2e$ being the flux quantum, C_J the junction capacitance, I_b the bias current, and I_c the critical current. The modes of all the TLRs couple to the transition $|e\rangle \leftrightarrow |f\rangle$, but decouple with other transitions, which could be realized by adjusting the d-spacing of the CBJJ quantum bits in advance. In terms of the superconducting quantum bits, the level measurement spacing could be adjusted conveniently by changing the external parameters' junction capacitance C_J , bias current I_b , and critical current I_c [21–24]. Those thoroughly describe how you can make the independent energy level be unaffected by the resonator, while also adjusting the energy level in advance spacing [25,26]. If the parameters of the CBJJ are $C_J = 71.5$ pF, $C_c = 60$ fF, $I_c = 67$ μ A, and $I_b / I_c \approx 0.99$, the transition frequency $\omega_{fe} / 2\pi = 2.853$ GHz. Therefore, if the TLR with the inductance $L_t^j = 75$ nH, capacitance $C_t^j = 2$ pF, and the full-wave frequency of the TLR is $\omega_c^j / 2\pi = 2.582$ GHz, the detuning $\omega_{fe} - \omega_c^j = 0.00628$ GHz $\ll 1$ GHz, and using rotating-wave approximation (RWA), the interacting Hamiltonian between the j th TLR and CBJJ is obtained as follows:

$$H_{T-C}^j = \eta_{t-c}^j \left(\sigma_{fe}^+ a_j e^{i\phi_j t} + \sigma_{fe}^- a_j^\dagger e^{-i\phi_j t} \right), \quad (2)$$

where η_{t-c}^j is the coupling factor, $\sigma_{fe}^+ = |f\rangle\langle e|$, $\sigma_{fe}^- = |e\rangle\langle f|$, and $\phi_j = \omega_{fe} - \omega_c^j$ is the detuning between $|e\rangle \leftrightarrow |f\rangle$ transition of the CBJJ and the j th TLR. Taking advantage of standard quantum optical technology, from Equations (2) to (3), if the parameters are $\eta_{t-c}^j / 2\pi \sim 100$ MHz and $\phi_j / 2\pi \sim 1000$ MHz, the large-detuning condition is realized in the experiment. The effective Hamiltonian can be obtained from Equation (2). The frequency ω_{fe} of the CBJJ and the mode frequency of the j th TLR, that is, $\phi_j \gg \eta_{t-c}^j$, it could be realized by adjusting the level-spacing of the CBJJ quantum bits. For CBJJ quantum bits, the level-spacing could be adjusted easily by adjusting the current bias or the magnetic flux bias [21–26]. The valid Hamiltonian between the j th TLR and CBJJ is [27]:

$$H_{T-C}^j = \sum_{j=1}^4 \frac{(\eta_{t-c}^j)^2}{\phi_j} (|f\rangle\langle f| - |e\rangle\langle e|) a_j^\dagger a_j. \quad (3)$$

2.2. N-V Center–TLR Resonant Interaction

As shown in Figure 1c, the ground state 3A and the first excited state 3E of the N-V center are the electron spin triplet state ($S = 1$). In the system, quantum bits are encoded into the ground triplet state—that is, $|^3A, m_s = 0\rangle = |0\rangle$ and $|^3A, m_s = \pm 1\rangle = |1\rangle$. Then, the Hamiltonian of the j th N-V center is:

$$H_{N-V}^j = \frac{1}{2} \omega_{10}^j S_j^z, \quad (4)$$

where $S_j^z = |1\rangle_j\langle 1| - |0\rangle_j\langle 0|$. If the TLRs(1,2,3,4) with the inductance $F_t^j = 68$ nH, capacitance $C_t^j = 1.8$ pF, the full-wave frequency of the TLR is $\omega_c^j/2\pi = 2.8583$ GHz, and the N-V center transition frequency $\omega_{10}^j/2\pi = 2.87$ GHz, the detuning $\omega_{10}^j - \omega_c^j = 0.073$ GHz $\ll 1$ GHz, and with RWA, the interaction Hamiltonian of the j th N-V center interacts with the j th TLR, described by:

$$H_{T-NV}^j = g_{t-NV}^j \left(S_j^+ a_j e^{i\delta_j t} + S_j^- a_j^\dagger e^{-i\delta_j t} \right), \quad (5)$$

where $S_j^+ = |1\rangle_j\langle 0|$ and $S_j^- = |0\rangle_j\langle 1|$. With g_{t-NV}^j as the j th N-V-TLR coupling strength, $\delta_j = \omega_{10}^j - \omega_c^j$ is the detuning between the j th N-V center transition frequency and the j th TLR frequency. When the frequency of the j th TLR is resonant with the j th N-V center, that is, $\omega_{10}^j = \omega_c^j$, Equation (5) becomes:

$$H_{T-NV}^j = g_{t-NV}^j \left(S_j^+ a_j + S_j^- a_j^\dagger \right). \quad (6)$$

2.3. CBJJ-TLR-N-V Center Off-Resonant Interaction

The mode of each TLR couples to the transition $|g\rangle \leftrightarrow |e\rangle$ of CBJJ, but decouples with other transitions. This could be realized by adjusting the frequency of each TLR, or by adjusting the level-spacing of the CBJJ quantum bits. The cavity mode frequency of the TLR can be changed in various experiments [28–32]. In terms of CBJJ quantum bits, the electron level spacing could be adjusted easily by adjusting the external controlled variables [33]. If the parameters of the CBJJ as $C_J = 71.5$ pF, $C_c = 60$ fF, $I_c = 67$ μ A, and $I_b/I_c \approx 0.99$, the transition frequency $\omega_{eg}/2\pi = 2.87$ GHz, the TLR with the inductance $F_t^j = 68$ nH, capacitance $C_t^j = 1.8$ pF, and the full-wave frequency of the TLR is $\omega_c^j/2\pi = 2.8583$ GHz, the detuning $\omega_{eg} - \omega_c^j = 0.073$ GHz $\ll 1$ GHz, with RWA, the interacting Hamiltonian between the j th TLR and CBJJ is:

$$H_{T-C}^j = g_{t-c}^j \left(\sigma_{eg}^+ a_j e^{i\Delta_j t} + \sigma_{eg}^- a_j^\dagger e^{-i\Delta_j t} \right), \quad (7)$$

where $\sigma_{eg}^+ = |e\rangle\langle g|$ and $\sigma_{eg}^- = |g\rangle\langle e|$. We used g_{t-c}^j as the j th CBJJ-TLR coupling strength, and $\Delta_j = \omega_{eg} - \omega_c^j$ as the detuning between the $|g\rangle \leftrightarrow |e\rangle$ transition frequency of CBJJ and the j th TLR frequency.

Combining Formulas (5) and (7), the total Hamiltonian can be obtained as follows:

$$H_I = \sum_{j=1}^4 \left[g_{t-c}^j \left(\sigma_{eg}^+ a_j e^{i\Delta_j t} + \sigma_{eg}^- a_j^\dagger e^{-i\Delta_j t} \right) + g_{t-NV}^j \left(S_j^+ a_j e^{i\delta_j t} + S_j^- a_j^\dagger e^{-i\delta_j t} \right) \right]. \quad (8)$$

Similarly to the analysis from Equations (2) to (3), from Equations (8) to (9), the large-detuning conditions by tuning the parameters of the CBJJ and TLR, that is, $\delta_j \gg g_{t-NV}^j$ and $\Delta_j \gg g_{t-c}^j$ can be achieved. There is a detailed discussion in Section 5, which can be achieved by changing the frequency of each TLR. The cavity mode frequency of the TLR can be changed in various experiments [28–33]. With this restriction, both N-V centers and CBJJ dispersively interact with TLRs, where it is convenient to remove the modes of TLRs by the intermediate states [18,19]. Using Frohlich's transformation method [20,27,34], the effective Hamiltonian from Equation (8) can be achieved.

$$H_{eff} = \sum_{j=1}^4 \lambda_j \left(\sigma_{eg}^- S_j^+ + \sigma_{eg}^+ S_j^- \right), \quad (9)$$

where $\lambda_j = g_{t-c}^j g_{t-NV}^j (\Delta_j + \delta_j) / 4\Delta_j \delta_j$ is the effective coupling strength between the j th N-V center and CBJJ.

3. Implementation of a Multipurpose Quantum Simulator

A two-qubit controlled-phase gate and the controlled-phase gate will realize the universal QCM. The CBJJ qubit is the control qubit, and the N-V center qubit is the target qubit. The controlled-phase gate can be realized in the following three steps:

Step (i): The j th N-V center and the j th TLR undergo an evolution for an interaction time $t_1 = \pi/(2g)$ under the Hamiltonian (6). Without loss of generality, all the N-V center–TLR resonant coupling strengths are identical—that is, $g_{t-NV}^j = g$ for $i = 1, 2, 3, 4$. It undergoes a transformation $|1\rangle_j|0\rangle_{c,j} \rightarrow -i|0\rangle_j|1\rangle_{c,j}$, with $(|0\rangle_{c,j})$ $|1\rangle_{c,j}$ representing a (zero) single-photon state of the j th TLR.

Step (ii): Adjust the parameters of TLRs(1,2,3,4) such that each of the N-V centers is decoupled from its own TLR, and adjust the parameters of CBJJ and TLRs(1,2,3,4) to satisfy the conditions of Equation (3). An interaction time $t_2 = (\pi\phi_j)/(\eta_{t-c}^j)^2$ will result in the transformation $|e\rangle|1\rangle_{c,j} \rightarrow -|e\rangle|1\rangle_{c,j}$.

Step (iii): Adjust the parameters of CBJJ so that it is decoupled from every TLR. The parameters of TLRs(1,2,3,4), such that each N-V center is resonant with its own TLR for an interaction time $t_3 = (3\pi)/(2g)$ will result in the transformation $|0\rangle_j|1\rangle_{c,j} \rightarrow i|1\rangle_j|0\rangle_{c,j}$.

The states after each step of the three transformations are summarized below:

$$\begin{array}{cccc}
 |g\rangle|0\rangle_j|0\rangle_{c,j} & |g\rangle|0\rangle_j|0\rangle_{c,j} & |g\rangle|0\rangle_j|0\rangle_{c,j} & |g\rangle|0\rangle_j|0\rangle_{c,j} \\
 |g\rangle|1\rangle_j|0\rangle_{c,j} \xrightarrow{\text{Step(i)}} & -i|g\rangle|0\rangle_j|1\rangle_{c,j} \xrightarrow{\text{Step(ii)}} & -i|g\rangle|0\rangle_j|1\rangle_{c,j} \xrightarrow{\text{Step(iii)}} & |g\rangle|1\rangle_j|0\rangle_{c,j} \\
 |e\rangle|0\rangle_j|0\rangle_{c,j} & |e\rangle|0\rangle_j|0\rangle_{c,j} & |e\rangle|0\rangle_j|0\rangle_{c,j} & |e\rangle|0\rangle_j|0\rangle_{c,j} \\
 |e\rangle|1\rangle_j|0\rangle_{c,j} & -i|e\rangle|0\rangle_j|1\rangle_{c,j} & i|e\rangle|0\rangle_j|1\rangle_{c,j} & -|e\rangle|1\rangle_j|0\rangle_{c,j}
 \end{array} \quad (10)$$

The auxiliary qubit and the j th TLR were decoupled from the other qubits at the end of the evolution.

Next, a universal QCM with our system required the following six steps:

Step (i): Suppose CBJJ and the four N-V centers do not couple with the four TLRs at the beginning. Meanwhile, suppose N-V center(1) carries the quantum states to be cloned, which are all recombination coefficients and are initially in an arbitrary superposed state. It is prepared in an arbitrary superposition state:

$$|\Psi\rangle_1 = \alpha|+\rangle_1 + \beta e^{i\varphi}|-\rangle_1, \quad (11)$$

where α and β are real coefficients, and they satisfy the normalization condition $\alpha^2 + \beta^2 = 1$, $\varphi \in (0, 2\pi)$, $|+\rangle_1 = 1/\sqrt{2}(|0\rangle_1 + |1\rangle_1)$, $|-\rangle_1 = 1/\sqrt{2}(|0\rangle_1 - |1\rangle_1)$. This state can be prepared by an additional microwave pulse acting on N-V center(1).

Suppose CBJJ is in the state $|g\rangle$ at the beginning, where the following operation could be adopted: add a classic pulse resonance $|g\rangle \rightarrow |e\rangle$ to realize interconversion, adjust the duration time t of the classic pulse, and set the auxiliary phase of the classic pulse; then, the CBJJ preparation state could be expressed as [35,36]:

$$|\Psi\rangle_2' = \cos \Omega t |g\rangle - i e^{-i\zeta} \sin \Omega t |e\rangle, \quad (12)$$

where Ω , ζ , and t are the Rabi frequency, initial phase, and duration of the pulse, respectively. If $\zeta = \pi$, Equation (12) can be written as:

$$|\Psi\rangle_2 = \cos \Omega t |g\rangle + i \sin \Omega t |e\rangle. \quad (13)$$

If N-V center(2) is initially in the state $|0\rangle_2$, the external parameters of the CBJJ and TLR(2) will meet the conditions of Equation (9), that is, $\delta_2 \gg g_{t-NV}^2$ and $\Delta_2 \gg g_{t-c}^2$. Therefore, the corresponding time evolution is:

$$\begin{aligned} |g\rangle|0\rangle_2 &\longrightarrow |g\rangle|0\rangle_2, \\ |g\rangle|1\rangle_2 &\longrightarrow \cos(\lambda_2 t) |g\rangle|1\rangle_2 - i \sin(\lambda_2 t) |e\rangle|0\rangle_2, \\ |e\rangle|0\rangle_2 &\longrightarrow \cos(\lambda_2 t) |e\rangle|0\rangle_2 - i \sin(\lambda_2 t) |g\rangle|1\rangle_2, \\ |e\rangle|1\rangle_2 &\longrightarrow |e\rangle|1\rangle_2. \end{aligned} \quad (14)$$

If the controlled-phase gate is between CBJJ and N-V center(1), then the state vector of the entangled N-V center-CBJJ state can be expressed as:

$$\begin{aligned} &\cos(\Omega t) (\alpha|+\rangle_1 + \beta e^{i\varphi}|-\rangle_1) |g\rangle|0\rangle_2 \\ &+ i \sin(\Omega t) (\alpha|-\rangle_1 + \beta e^{i\varphi}|+\rangle_1) [\cos(\lambda_2 t) |e\rangle|0\rangle_2 \\ &- i \sin(\lambda_2 t) |g\rangle|1\rangle_2]. \end{aligned} \quad (15)$$

Step (ii): Adjust the parameters of CBJJ and TLR(2) to make them return to the initial state, where the CBJJ and N-V center(2) is decoupling with TLR(2). Then, when the N-V center(3) is on the state $|0\rangle_3$ at the beginning, adjust the external parameters of CBJJ and TLR(3), as well as when the corresponding time evolution is also Equation (9)—that is, $\delta_3 \gg g_{t-NV}^3$ and $\Delta_3 \gg g_{t-c}^3$. In case the evolution time selected $t_4 = \pi/(2\lambda_3)$, the generated state is:

$$\begin{aligned} &\cos(\Omega t) (\alpha|+\rangle_1 + \beta e^{i\varphi}|-\rangle_1) |g\rangle|0\rangle_2|0\rangle_3 + \\ &i \sin(\Omega t) (\alpha|-\rangle_1 + \beta e^{i\varphi}|+\rangle_1) [-i \cos(\lambda_2 t) |g\rangle|0\rangle_2|1\rangle_3 \\ &- i \sin(\lambda_2 t) |g\rangle|1\rangle_2|0\rangle_3]. \end{aligned} \quad (16)$$

Step (iii): The classic $\pi/2$ micro-wave pulse on N-V center(1,2,3) and the transformation generated by the pulse could be written as:

$$\begin{aligned} |0\rangle_j &\leftrightarrow \sqrt{\frac{1}{2}} (|0\rangle_j - |1\rangle_j) = |-\rangle_j, \\ |1\rangle_j &\leftrightarrow \sqrt{\frac{1}{2}} (|0\rangle_j + |1\rangle_j) = |+\rangle_j, \end{aligned} \quad (17)$$

where $j = 1, 2, 3$. Then, the total state of N-V center(1,2,3) and CBJJ is:

$$\begin{aligned} &\mathcal{A} (\alpha|1\rangle_1 + \beta e^{i\varphi}|0\rangle_1) |g\rangle|-\rangle_2|-\rangle_3 \\ &+ \mathcal{B} (\alpha|0\rangle_1 + \beta e^{i\varphi}|1\rangle_1) |g\rangle|-\rangle_2|+\rangle_3 \\ &+ \mathcal{C} (\alpha|0\rangle_1 + \beta e^{i\varphi}|1\rangle_1) |g\rangle|+\rangle_2|-\rangle_3, \end{aligned} \quad (18)$$

where $\mathcal{A} = \cos(\Omega t)$, $\mathcal{B} = \sin(\Omega t) \cos(\lambda_2 t)$, and $\mathcal{C} = \sin(\Omega t) \sin(\lambda_2 t)$.

Step (iv): Adjust the parameters of CBJJ and TLR(3) to make them return to the initial state, where the CBJJ and N-V center(3) are decoupling with TLR(3). Then, adjust the external parameters of

CBJJ and TLR(1) to make it satisfy Equation (9)—that is, $\delta_1 \gg g_{t-NV}^1$ and $\Delta_1 \gg g_{t-c}^1$, and the evolution time is selected as $t_5 = (3\pi)/(2\lambda_1)$, where the generated state is:

$$\begin{aligned} & \mathcal{A} \left(\alpha |e\rangle + \beta e^{i\varphi} |g\rangle \right) |0\rangle_1 |-\rangle_2 |-\rangle_3 \\ & + \mathcal{B} \left(\alpha |g\rangle + \beta i e^{i\varphi} |e\rangle \right) |0\rangle_1 |-\rangle_2 |+\rangle_3 \\ & + \mathcal{C} \left(\alpha |g\rangle + \beta i e^{i\varphi} |e\rangle \right) |0\rangle_1 |+\rangle_2 |-\rangle_3. \end{aligned} \quad (19)$$

Step (v): Adjust the parameters of CBJJ and TLR(1) to make them return to the initial state, and implement a controlled-phase gate on N-V center(2,3). The basis $\{|+\rangle, |-\rangle\}$ vector is the implemented controlled-NOT gate, and the generated state is:

$$\begin{aligned} & \mathcal{A} \left(\alpha |e\rangle |+\rangle_2 |+\rangle_3 + \beta e^{i\varphi} |g\rangle |-\rangle_2 |-\rangle_3 \right) |0\rangle_1 \\ & + \mathcal{B} \left(\alpha |g\rangle |-\rangle_2 |+\rangle_3 + \beta i e^{i\varphi} |e\rangle |+\rangle_2 |-\rangle_3 \right) |0\rangle_1 \\ & + \mathcal{C} \left(\alpha |g\rangle |+\rangle_2 |-\rangle_3 + \beta i e^{i\varphi} |e\rangle |-\rangle_2 |+\rangle_3 \right) |0\rangle_1. \end{aligned} \quad (20)$$

Step (vi): Adjust TLRs(1,2,3,4), as well as the parameters of the corresponding N-V center(1,2,3,4) to make them return to the initial state. Suppose N-V center(4) is on the state $|0\rangle_4$, and adjust the external parameters of CBJJ and TLR(4) to make them satisfy the conditions required by Equation (9), that is, $\delta_4 \gg g_{t-NV}^4$ and $\Delta_4 \gg g_{t-c}^4$. If the evolution time is selected as $t_6 = \pi/(2\lambda_4)$, through simple arrangement, the final state of the overall system could be written as:

$$\begin{aligned} & \alpha [\mathcal{A} |+\rangle_2 |+\rangle_3 |\mathcal{N}\rangle + |\mathcal{N}_\perp\rangle (\mathcal{B} |-\rangle_2 |+\rangle_3 + \mathcal{C} |+\rangle_2 |-\rangle_3)] \\ & + \beta e^{i\varphi} [\mathcal{A} |-\rangle_2 |-\rangle_3 |\mathcal{N}_\perp\rangle + |\mathcal{N}\rangle (\mathcal{B} |+\rangle_2 |-\rangle_3 + \mathcal{C} |-\rangle_2 |+\rangle_3)], \end{aligned} \quad (21)$$

where $|\mathcal{N}\rangle = |g\rangle|0\rangle_1|1\rangle_4$, $|\mathcal{N}_\perp\rangle = |g\rangle|0\rangle_1|0\rangle_4$. The N-V center(4) in Equation (21) ensures the orthogonality of the states $|\mathcal{N}\rangle$ and $|\mathcal{N}_\perp\rangle$; therefore, it is the most important qubit in the ancillary qubit state. The state of Equation (21) is $|\Psi\rangle$, the N-V center state $|+\rangle$, and the ancillary state $|\mathcal{N}\rangle$ has the same quantum logic state. In Equation (21), the second and the third N-V center qubit is the clone qubit, and the corresponding fidelities is:

$$\begin{aligned} F_2 &= \langle \Psi | Tr_{1,3,4,CBJJ} (|\Psi\rangle\langle\Psi|) | \Psi \rangle \\ &= \left(\alpha^4 + \beta^4 \right) \left(\mathcal{A}^2 + \mathcal{C}^2 \right) + \alpha^2 \beta^2 \left(2\mathcal{B}^2 + 4\mathcal{A}\mathcal{C} \right), \\ F_3 &= \langle \Psi | Tr_{1,2,4,CBJJ} (|\Psi\rangle\langle\Psi|) | \Psi \rangle \\ &= \left(\alpha^4 + \beta^4 \right) \left(\mathcal{A}^2 + \mathcal{B}^2 \right) + \alpha^2 \beta^2 \left(2\mathcal{C}^2 + 4\mathcal{A}\mathcal{B} \right). \end{aligned} \quad (22)$$

The different QCM was realized in this quantum simulator. A universal QCM can be obtained when the coefficients α , β , and φ are unknown. The fidelities $F_2 = F_3 = 5/6$ can be obtained if $\Omega t = \arccos(\sqrt{2/3})$, $\lambda_2 t_7 = \pi/4$ from Equation (22). Then, an optimal symmetric $1 \rightarrow 2$ universal QCM is realized. If the variables Ωt and $\lambda_2 t$ satisfy the relationship $\tan \Omega t (\cos \lambda_2 t + \sin \lambda_2 t) = 1$, the fidelities can be written as $F_2 = (1 + \sin 2\lambda_2 t + \sin^2 \lambda_2 t) / (2 + \sin 2\lambda_2 t)$, $F_3 = (1 + \sin 2\lambda_2 t + \cos^2 \lambda_2 t) / (2 + \sin 2\lambda_2 t)$, which are shown in Figure 2a. Then, the state of Equation (21) is the transformation of optimal asymmetric universal quantum cloning [37]. The phase-covariant QCM is realized if the coefficients α , β are known, and φ is unknown. With $\alpha = \cos \frac{Y}{2}$, $\beta = \sin \frac{Y}{2}$ ($Y \in [0, 2\pi]$), $\lambda_2 t = \pi/4$, and $\cos \Omega t = \sqrt{(1 + 1/\sqrt{1 + 2 \tan^4 Y})}/2$, the state of Equation (21) is the transformation of optimal phase-covariant quantum cloning [10,11]. The fidelities can be calculated as $F_2 = F_3 = (2 + \cos^2 Y + \sqrt{\cos^4 Y + 2 \sin^4 Y})/4$, which is shown in Figure 2b. If $Y = \pi/2$, $\cos \Omega t = \sqrt{1/2}$, $\alpha = \beta = 1/\sqrt{2}$, the state of Equation (21) is the transformation of

optimal symmetric phase-covariant quantum cloning, and N-V center(1) is in the equatorial state $(|+\rangle_1 + e^{i\varphi}|-\rangle_1)/\sqrt{2}$, which is to be cloned, and the two fidelities are $F_2 = F_3 = (1 + 1/\sqrt{2})/2$. If $\lambda_2 t \in [0, \pi/2]$, the state of Equation (21) is the transformation of optimal asymmetric phase-covariant quantum cloning, and the two fidelities are $F_2 = (1 + \sin \lambda_2 t)/2, F_3 = (1 + \cos \lambda_2 t)/2$, which is shown by the dashed lines in Figure 2a. The optimal asymmetric phase-covariant quantum cloning has a higher fidelity than the optimal asymmetric universal quantum cloning from Figure 2a. Based on the above analysis, the high-fidelity quantum cloning can be realized by suitable parameters in the quantum simulator.

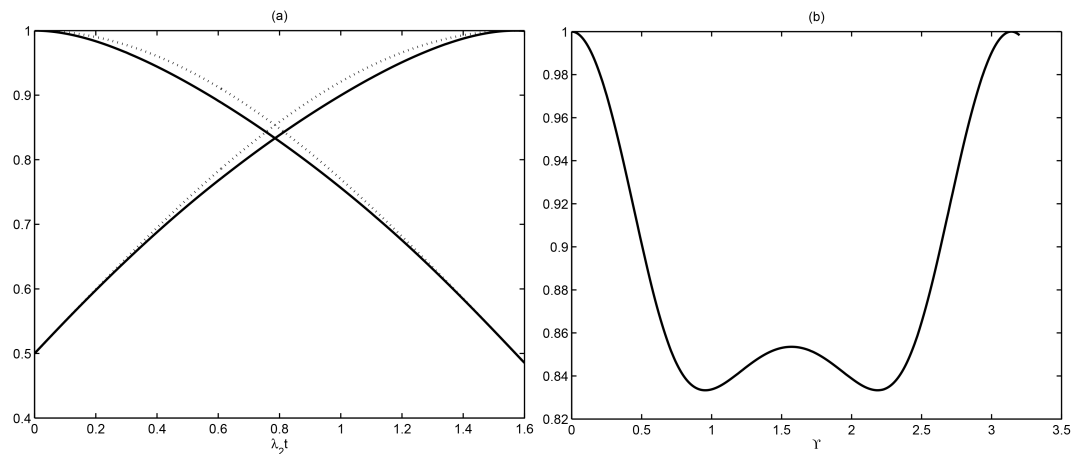


Figure 2. (a) The two solid lines are the fidelities of the optimal asymmetric universal quantum cloning, and the two dashed lines are the fidelities of the optimal asymmetric phase-covariant quantum cloning. (b) The fidelity of the optimal phase-covariant quantum cloning.

4. Implementation of Quantum Anticloning

With an excitation number operator $\mathcal{M} = \sigma_{eg}^+ \sigma_{eg}^- + \sum_{j=1}^4 S_j^+ S_j^-$ [26], $[H_{eff}, \mathcal{M}] = 0$, the eigenvalue is $M = 0$, and $M = 1$ of \mathcal{M} , and the basic states are:

$$\begin{aligned}
 |\chi_0\rangle &= |0_1 0_2 0_3 0_4 g\rangle = |q_0\rangle \otimes |g\rangle, \\
 |\chi_1\rangle &= |1_1 0_2 0_3 0_4 g\rangle = |q_1\rangle \otimes |g\rangle, \\
 |\chi_2\rangle &= |0_1 1_2 0_3 0_4 g\rangle = |q_2\rangle \otimes |g\rangle, \\
 |\chi_3\rangle &= |0_1 0_2 1_3 0_4 g\rangle = |q_3\rangle \otimes |g\rangle, \\
 |\chi_4\rangle &= |0_1 0_2 0_3 1_4 g\rangle = |q_4\rangle \otimes |g\rangle, \\
 |\chi_5\rangle &= |0_1 0_2 0_3 0_4 e\rangle = |q_0\rangle \otimes |e\rangle,
 \end{aligned} \tag{23}$$

where $|\chi_0\rangle$ denotes the state in the subspace with eigenvalue $M = 0$, and $|\chi_1\rangle \cdots |\chi_5\rangle$ denotes the states in the subspace with eigenvalue $M = 1$. Assume $|\psi(0)\rangle$ is the initial state of this system, with time t , and the state of this system evolves into $|\psi(t)\rangle = \hat{U}(t)|\psi(0)\rangle$, where $\hat{U}(t)$ is the time evolution operator in the basis of states $|\chi_1\rangle \cdots |\chi_5\rangle$, where it has the form:

$$\hat{U}(t) = \begin{pmatrix} 1 - 2\lambda_1^2 \epsilon & -2\lambda_1 \lambda_2 \epsilon & -2\lambda_1 \lambda_3 \epsilon & -2\lambda_1 \lambda_4 \epsilon & -i\lambda_1 \sin(vt)/v \\ -2\lambda_2 \lambda_1 \epsilon & 1 - 2\lambda_2^2 \epsilon & -2\lambda_2 \lambda_3 \epsilon & -2\lambda_2 \lambda_4 \epsilon & -i\lambda_2 \sin(vt)/v \\ -2\lambda_3 \lambda_1 \epsilon & -2\lambda_3 \lambda_2 \epsilon & 1 - 2\lambda_3^2 \epsilon & -2\lambda_3 \lambda_4 \epsilon & -i\lambda_3 \sin(vt)/v \\ -2\lambda_4 \lambda_1 \epsilon & -2\lambda_4 \lambda_2 \epsilon & -2\lambda_3 \lambda_4 \epsilon & 1 - 2\lambda_4^2 \epsilon & -i\lambda_4 \sin(vt)/v \\ -i\lambda_1 \sin(vt)/v & -i\lambda_2 \sin(vt)/v & -i\lambda_3 \sin(vt)/v & -i\lambda_4 \sin(vt)/v & \cos(vt) \end{pmatrix}, \tag{24}$$

where $v^2 = \sum_{j=1}^4 \lambda_j^2$ is the effective collective Rabi oscillation frequency of the four N-V centers, $\epsilon = \sin^2(vt/2)/v^2$.

Next, the quantum anticloning with this temporal evolution equation required the following three steps:

Step (i): Assume that the CBJJ and the four N-V centers are initially decoupled from the four TLRs. We also assumed that the N-V center(1) carried the quantum state, which was to be anticloned. It was prepared in an arbitrary coherent superposition state, $\frac{1}{\sqrt{2}}(|0_1\rangle + e^{i\zeta}|1_1\rangle)$. The CBJJ qubit and the other three N-V center qubits were in their unexcited states, $|0_20_30_4g\rangle$. Therefore, the initial state of this system is:

$$\begin{aligned} |\psi(0)\rangle &= \frac{1}{\sqrt{2}} \left(|0_1\rangle + e^{i\zeta} |1_1\rangle \right) \otimes |0_20_30_4g\rangle \\ &= \frac{1}{\sqrt{2}} \left(|\chi_0\rangle + e^{i\zeta} |\chi_1\rangle \right). \end{aligned} \quad (25)$$

Step (ii): Adjust the external parameters of CBJJ and the four TLRs to meet the conditions of Equation (9)—that is, $\delta_j \gg g_{t-NV}^j$ and $\Delta_j \gg g_{t-c}^j$, where $j = 1, 2, 3, 4$. Using Equation (23), the initial state $|\psi(0)\rangle$ becomes:

$$|\psi(t)\rangle = \frac{1}{\sqrt{2}} \left(|\chi_0\rangle + e^{i\zeta} |\chi_1(t)\rangle \right), \quad (26)$$

where

$$|\chi_1(t)\rangle = \sum_{j=1}^4 U_{j1}(t) |q_j\rangle \otimes |g\rangle - i \frac{\lambda_1 \sin(vt)}{v} |\chi_5\rangle. \quad (27)$$

If the evolution time is $t = t^* = \frac{n\pi}{v}$ (n is an odd number), the CBJJ is separable from the N-V centers. When the CBJJ state notation is dropped, the final state at $t = t^*$ will be:

$$|\psi(t^*)\rangle = \frac{1}{\sqrt{2}} \left[|q_0\rangle + e^{i\zeta} \left(b_1 |q_1\rangle + b \sum_{j=2}^4 |q_j\rangle \right) \right], \quad (28)$$

where

$$b_1 = \frac{3 - r^2}{3 + r^2}, \quad b = \frac{-2r}{3 + r^2}. \quad (29)$$

In Equation (28), $\lambda_1 \neq \lambda_2 = \lambda_3 = \lambda_4 = \lambda$, and where $r = \lambda_1/\lambda$, the effective collective Rabi oscillation frequency was $v = \lambda\sqrt{r^2 + 3}$.

Step (iii): If $b_1 = \pm b$, and the optimal coupling ratio $r_+ = 3, r_- = 1$, Equation (27) can be written as:

$$|\psi(t^*)\rangle = \frac{1}{\sqrt{2}} \left(|q_0\rangle + e^{i\zeta} |W_4^\pm\rangle \right), \quad (30)$$

where $|W_4^\pm\rangle = -\frac{1}{2} \left(\pm |q_1\rangle + \sum_{j=2}^4 |q_j\rangle \right)$. So far, it achieved phase-covariant quantum anticloning, and prepared a $|W_4^\pm\rangle$ entangled state [38,39].

5. Discussion

The feasibility of the experiment was discussed in the presented scheme. The method in our system requires different conditions to realize different quantum clonings. For example, if $\eta_{t-c}^j/2\pi \sim 100$ MHz, $\phi_j/2\pi \sim 1000$ MHz [40], and the off-resonant condition $\phi_j \gg \eta_{t-c}^j$, the CBJJ-TLR off-resonant case is satisfied; whereas if the j th TLR with inductance $F_t^j = 60.7$ nH, capacitance $C_t^j = 2$ pF,

the full-wave frequency $\omega_c^j/2\pi = 2.87$ GHz [41], it is equal to zero-field splitting $D_{gs}/2\pi = 2.87$ GHz between the lowest level $m_s = 0$, the degenerated level $m_s = \pm 1$ [30], and the N-V center–TLR resonant condition $\omega_{10}^j = \omega_c^j$, where the N-V center–TLR resonant case is satisfied. If the parameters of the j th TLR is assumed as inductance $F_t^j = 70$ nH and capacitance $C_t^j = 2$ pF, the frequency $\omega_c^j/2\pi = D_{gs} - \delta_j = 2.67$ GHz, the detuning $\delta_j/2\pi = 200$ MHz [42], the parameters of CBJJ is tuned as $C_j = 2.3$ pF, $C_c = 1$ fF, $I_c = 2.177$ μ A, $I_b/I_c \approx 0.99$, the detuning $\Delta_j/2\pi = 250$ MHz, and the coupling factors $g_{t-c}^j/2\pi = 50$ MHz [41], then the CBJJ–TLR–N-V center off-resonant case is satisfied. There are some schemes to realize the strong coupling between individual N-V centers and a TLR [43,44], which could create a N-V center–TLR interaction with a strength of tens of MHz. Then, if $g_{t-NV}^j/2\pi = 50$ MHz [41], $\delta_j \gg g_{t-NV}^j$ and $\Delta_j \gg g_{t-c}^j$, for the CBJJ–TLR–N-V center off-resonant case the CBJJ–TLR–N-V center off-resonant conditions are satisfied. Therefore, the considerable effective coupling strength between the j th N-V center and CBJJ are $\lambda_j/2\pi = g_{t-c}^j g_{t-NV}^j (\Delta_j + \delta_j) / 4\Delta_j \delta_j \approx 35$ MHz.

For the process of quantum anti-cloning, the optimal coupling ratio $r_+ = 3, r_- = 1$ could be obtained by controlling the position of the N-V centers with respect to the TLR. Such as for the coupling ratio $r_- = 1$, this could be realized by placing the four N-V centers in the equivalent positions with respect to the TLR. For the coupling ratio $r_+ = 3$, this could be realized by placing the three output qubits N-V centers(2,3,4) in equivalent positions, where the input qubit N-V center(1) is placed elsewhere to guarantee $r_+ = 3$.

In the current experiments, the TLR decay rate κ , the spontaneous emission rate γ_{fe} (γ_{eg}), and quantum tunneling rate Γ_f (Γ_e) of the level $|f\rangle$ ($|e\rangle$) of CBJJ, the dephasing rate γ_ϕ of CBJJ were on the order of hundreds of kilohertz [45,46]. Because all the coupling strengths η , g , and λ were two orders higher than the dissipation rates, the scheme can be said to be reliable and feasible. On the other hand, the relaxation time T_1 of the N-V centers were reported from 6 ms at room temperature [47] to 28 – 265 s at low temperature [48]. In addition, the dephasing time $T_2 = 2$ ms of the N-V centers was also reported [49]. In the process of universal quantum cloning, the operation time in every step was $t_1 \sim 5$ ns, $t_2 \sim 50$ ns, $t_3 \sim 15$ ns, $t_4 \sim 3.6$ ns, $t_5 \sim 7.2$ ns, and $t_6 \sim 21.6$ ns, which was much shorter than the decoherence times of the N-V center, TLR, and CBJJ. In the process of phase-covariant quantum anti-cloning, the evolution time can be calculated as $t = t^* = \frac{\pi}{v} \sim 7.14$ ns, which is much shorter than the decoherence times of the N-V center, TLR, and CBJJ. The implementation of a multipurpose quantum simulator for high-fidelity quantum cloning and anti-cloning is feasible with the system.

6. Conclusions

As discussed in the Reference [4], the fidelity should have a precision greater than 0.92. In the scheme, all the CBJJ–NV interactions and classical pulses led to errors. The total operations were 10 when it considered the detection and preparation. Therefore, if the pulse has a fidelity greater than $\sqrt[10]{0.92} \approx 0.992$, the necessary precision can be satisfied. This value is smaller than the value (≈ 0.995) presented in the Reference [4], which could greatly reduce the experimental requirement for the pulse. In the process of quantum anti-cloning, if we chose the optimal coupling ratio $r_+ = 3, r_- = 1$, then the fidelity of m outputs would be $\frac{1}{2}(1 + \frac{1}{\sqrt{m}})$ [38]. In the system, if $m = 2$, then the maximal fidelity is $\frac{1}{2}(1 + \frac{1}{\sqrt{2}})$, where the optimal fidelity is 1 \rightarrow 2 for phase-covariant cloning [11]. It realized a multipurpose quantum simulator for high-fidelity quantum cloning and the anti-cloning of an equatorial state.

In summary, a novel system which could realize a multi-purpose quantum simulator was put forward in this paper, which can implement different quantum cloning and anti-clonings, including optimal symmetric universal quantum cloning, optimal asymmetric universal quantum cloning, optimal symmetric phase covariance quantum cloning, optimal asymmetric phase covariance quantum cloning, and optimal phase covariance quantum anti-cloning. Solid quantum bits were well-isolated with the external world, which could inhibit the decoherence and made it easy to operate. Moreover,

it features less operating procedures and auxiliary quantum bits, which could facilitate quantum cloning and anti-cloning and lower the experimental requirements of the system. Finally, after quantum cloning and anti-cloning, different quantum clones with various reliabilities can be obtained by pre-processing of the initial quantum state. Thus, the quantum resources can be used effectively, and the scheme is an economical one. Because of the short operation time and long decoherence time of N-V centers, TLRs and CBJJ, the two schemes are realizable with experimental conditions which are currently available.

Author Contributions: T.Y. gave the basic idea of the manuscript, Y.Z. wrote the main manuscript text, S.C., F.Z. and S.X. contributed to the discussion and introduction, K.S. implemented the modification of this paper in order to improve its quality. All authors read and approved the final manuscript.

Funding: This work was supported by National Natural Science Foundation of China under Grant (Nos. 11574081, 11374096 and 11074072).

Acknowledgments: The Natural Science Foundation of Hunan Province, China (No. 2017JJ2214).

Conflicts of Interest: The authors declare no conflict of interest.

References

1. Wootters, W.K.; Zurek, W.H. A single quantum cannot be cloned. *Nature* **1982**, *299*, 802. [[CrossRef](#)]
2. Buzek, V.; Hillery, M. Quantum copying: Beyond the no-cloning theorem. *Phys. Rev. A* **1996**, *54*, 1844. [[CrossRef](#)]
3. Duan, L.M.; Guo, G.C. A probabilistic cloning machine for replicating two non-orthogonal states. *Phys. Lett. A* **1998**, *243*, 261–264. [[CrossRef](#)]
4. Milman, P.; Ollivier, H.; Raimond, J.M. Universal quantum cloning in cavity QED. *Phys. Rev. A* **2003**, *67*, 57–63. [[CrossRef](#)]
5. Zou, X.B.; Pahlke, K.; Mathis, W. Scheme for the implementation of a universal quantum cloning machine via cavity-assisted atomic collisions in cavity QED. *Phys. Rev. A* **2003**, *67*, 024304. [[CrossRef](#)]
6. Ye, L.; Guo, G.C. Scheme for implementing quantum dense coding in cavity QED. *Phys. Rev. A* **2005**, *71*, 034304. [[CrossRef](#)]
7. Fang, B.L.; Wu, T.; Ye, L. Realization of a general quantum cloning machine via cavity-assisted interaction. *Europhys. Lett.* **2012**, *97*, 60002. [[CrossRef](#)]
8. Rui, P.S.; Zhang, W.; Liao, Y.L.; Zhang, Z.Y. Probabilistic quantum cloning of a subset of linearly dependent states. *Eur. Phys. J. D* **2018**, *72*, 26. [[CrossRef](#)]
9. Bruß, D.; DiVincenzo, D.P.; Ekert, A.; Fuchs, C.A.; Macchiavello, C.; Smolin, J.A. Optimal universal and state-dependent quantum cloning. *Phys. Rev. A* **1998**, *57*, 2368. [[CrossRef](#)]
10. Pan, X.Y.; Liu, G.Q.; Yang, L.L.; Fan, H. Solid-state optimal phase-covariant quantum cloning machine. *Appl. Phys. Lett.* **2011**, *99*, 051113. [[CrossRef](#)]
11. Bruss, D.; Cinchetti, M.; D’Ariano, G.M.; Macchiavello, C. Phase-covariant quantum cloning. *Phys. Rev. A* **2000**, *62*, 012302. [[CrossRef](#)]
12. Knoll, L.T.; Grande, I.H.; Larotonda, M.A. Photonic quantum simulator for unbiased phase covariant cloning. *Appl. Phys. B* **2018**, *124*, 3. [[CrossRef](#)]
13. Aguilar, J.C.; Misawa, M.; Matsuda, K.; Rehman, S.; Yasumoto, M.; Suzuki, Y.; Takeuchi, A.; Berriel-Valdos, L.R. Starlet transform applied to digital Gabor holographic microscopy. *Appl. Opt.* **2016**, *24*, 6617–6624. [[CrossRef](#)]
14. Meng, F.X.; Yu, X.T.; Zhang, Z.C. An economical state-dependent telecloning for a multiparticle GHZ state. *Quantum Inf. Process* **2018**, *17*, 66. [[CrossRef](#)]
15. Wu, H.J.; Zhao, J.; Zhu, A.D. Protection of Telecloning Over Noisy Channels with Environment-Assisted Measurements and Weak Measurements. *Int. J. Theor. Phys.* **2018**, *57*, 1235. [[CrossRef](#)]
16. Ma, P.C.; Chen, G.B.; Li, X.W.; Zhan, Y.B. Quantum jointly assisted cloning of an unknown three-dimensional equatorial state. *Laser Phys.* **2018**, *28*, 025201. [[CrossRef](#)]
17. Bouchard, F.; Fickler, R.; Boyd, R.; Karimi, E. High-dimensional quantum cloning and applications to quantum hacking. *Sci. Adv.* **2017**, *3*, e1601915. [[CrossRef](#)]

18. Bartkiewicz, K.; Černoč, A.; Chimczak, G.; Lemr, K.; Miranowicz, A.; Nori, F. Experimental quantum forgery of quantum optical money. *npj Quantum Inf.* **2017**, *7*, 1. [[CrossRef](#)]
19. Hu, Y.; Xiao, Y.F.; Zhou, Z.W.; Guo, G.C. Controllable coupling of superconducting transmission-line resonators. *Phys. Rev. A* **2007**, *75*, 012314. [[CrossRef](#)]
20. Clarke, J.; Cleland, A.N.; Devoret, M.H.; Esteve, D.; Martinis, J.M. Quantum mechanics of a macroscopic variable: the phase difference of a Josephson junction. *Science* **1988**, *239*, 992. [[CrossRef](#)]
21. You, J.Q.; Nori, F. Superconducting Circuits and Quantum Information. *Phys. Today* **2005**, *58*, 42–47. [[CrossRef](#)]
22. Neeley, M.; Ansmann, M.; Bialczak, R.C.; Hofheinz, M.; Katz, N.; Lucero, E.; O’Connell, A.; Wang, H.; Cleland, A.N.; Martinis, J.M. Process tomography of quantum memory in a Josephson-phase qubit coupled to a two-level state. *Nat. Phys.* **2008**, *4*, 523. [[CrossRef](#)]
23. Zagoskin, A.M.; Ashhab, S.; Johansson, J.R.; Nori, F. Quantum two-level systems in Josephson junctions as naturally formed qubits. *Phys. Rev. Lett.* **2006**, *97*, 077001. [[CrossRef](#)]
24. Xiong, S.J.; Zhang, Y.; Sun, Z.; Yu, L.; Su, Q.; Xu, X.Q.; Jin, J.S.; Xu, Q.J.; Chen, K.F.; Yang, C.P. Experimental simulation of a quantum channel without the rotating-wave approximation: Testing quantum temporal steering. *Optica* **2017**, *4*, 1065–1072. [[CrossRef](#)]
25. Yang, C.P.; Zheng, S.B.; Nori, F. Multiqubit tunable phase gate of one qubit simultaneously controlling n qubits in a cavity. *Phys. Rev. A* **2010**, *82*, 062326. [[CrossRef](#)]
26. Liu, Y.; You, J.Q.; Wei, L.F.; Sun, C.P.; Nori, F. Optical selection rules and phase-dependent adiabatic state control in a superconducting quantum circuit. *Phys. Rev. Lett.* **2005**, *95*, 087001. [[CrossRef](#)]
27. Guo, G.C.; Zheng, S.B. Generation of Schrödinger cat states via the Jaynes-Cummings model with large detuning. *Phys. Lett. A* **1996**, *223*, 332. [[CrossRef](#)]
28. Brune, M.; Hagle, E.; Dreyer, J.; Maitre, X.; Maali, A.; Wunderlich, C.; Raimond, J.M.; Haroche, S. Observing the progressive decoherence of the “meter” in a quantum measurement. *Phys. Rev. Lett.* **1996**, *77*, 4887. [[CrossRef](#)]
29. Sandberg, M.; Wilson, C.M.; Persson, F.; Bauch, T.; Johansson, G.; Shumeiko, V.; Duty, T.; Delsing, P. Tuning the field in a microwave resonator faster than the photon lifetime. *Appl. Phys. Lett.* **2008**, *92*, 203501. [[CrossRef](#)]
30. Palacios-Laloy, A.; Nguyen, F.; Mallet, F.; Bertet, P.; Vion, D.; Esteve, D. Tunable resonators for quantum circuits. *J. Low Temp. Phys.* **2008**, *151*, 1034–1042. [[CrossRef](#)]
31. Johansson, J.R.; Johansson, G.; Wilson, C.M.; Nori, F. Dynamical Casimir effect in a superconducting coplanar waveguide. *Phys. Rev. Lett.* **2009**, *103*, 147003. [[CrossRef](#)]
32. Liao, J.Q.; Gong, Z.R.; Zhou, L.; Liu, Y.X.; Sun, C.P.; Nori, F. Controlling the transport of single photons by tuning the frequency of either one or two cavities in an array of coupled cavities. *Phys. Rev. A* **2010**, *81*, 042304. [[CrossRef](#)]
33. Clarke, J.; Wilhelm, F.K. Superconducting quantum bits. *Nature* **2008**, *453*, 1031. [[CrossRef](#)]
34. Li, Y.; Bruder, C.; Sun, C.P. Quantum nondemolition measurements of photon number by atomic beam deflection. *Phys. Rev. Lett.* **2007**, *75*, 032302. [[CrossRef](#)]
35. Zhu, M.Z.; Ye, L. Implementing a quantum cloning machine in separate cavities via the optical coherent pulse as a quantum communication bus. *Phys. Rev. A* **2015**, *91*, 127901. [[CrossRef](#)]
36. Yang, C.P. Preparation of n-qubit Greenberger-Horne-Zeilinger entangled states in cavity QED: An approach with tolerance to nonidentical qubit-cavity coupling constants. *Phys. Rev. A* **2011**, *83*, 062302. [[CrossRef](#)]
37. Cerf, N.J. Asymmetric quantum cloning machines. *Opt. Acta Int. J. Opt.* **2004**, *47*, 187–209. [[CrossRef](#)]
38. Olaya-Castro, A.; Johnson, N.F.; Quiroga, L. Robust one-step catalytic machine for high fidelity anticloning and W-state generation in a multiqubit system. *Phys. Rev. Lett.* **2005**, *94*, 110502. [[CrossRef](#)]
39. Gisin, N.; Popescu, S. Spin flips and quantum information for antiparallel spins. *Phys. Rev. Lett.* **1999**, *83*, 432. [[CrossRef](#)]
40. DiCarlo, L.; Reed, M.D.; Sun, L.; Johnson, B.R.; Chow, J.M.; Gambetta, J.M.; Frunzio, L.; Girvin, S.M.; Devoret, M.H.; Schoelkopf, R.J. Preparation and measurement of three-qubit entanglement in a superconducting circuit. *Nature* **2010**, *467*, 574. [[CrossRef](#)]
41. Yang, W.L.; Yin, Z.Q.; Hu, Y.; Feng, M.; Du, J.F. High-fidelity quantum memory using nitrogen-vacancy center ensemble for hybrid quantum computation. *Phys. Rev. A* **2011**, *84*, 3442–3448. [[CrossRef](#)]

42. Manson, N.B.; Harrison, J.P.; Sellars, M.J. Nitrogen-vacancy center in diamond: Model of the electronic structure and associated dynamics. *Phys. Rev. B* **2006**, *74*, 104303. [[CrossRef](#)]
43. Gao, M.; Wu, C.W.; Deng, Z.J.; Zou, W.J.; Zhou, L.G.; Li, C.Z.; Wang, X.B. Controllable strong coupling between individual spin qubits and a transmission line resonator via nanomechanical resonators. *Phys. Lett. A* **2012**, *376*, 595. [[CrossRef](#)]
44. Jin, P.Q.; Marthaler, M.; Shnirman, A.; Schön, G. Strong coupling of spin qubits to a transmission line resonator. *Phys. Rev. Lett.* **2012**, *108*, 190506. [[CrossRef](#)]
45. Yu, Y. Coherent temporal oscillations of macroscopic quantum states in a Josephson junction. *Science* **2002**, *296*, 889–892. [[CrossRef](#)]
46. Zhao, Y.J.; Fang, X.M.; Zhou, F.; Song, K.H. A scheme for realizing quantum information storage and retrieval from quantum memory based on nitrogenvacancy centers. *Phys. Rev. A* **2012**, *86*, 052325. [[CrossRef](#)]
47. Neumann, P.; Mizuochi, N.; Rempp, F.; Hemmer, P.; Watanabe, H.; Yamasaki, S.; Jacques, V.; Gaebel, T.; Jelezko, F.; Wrachtrup, J. Multipartite entanglement among single spins in diamond. *Science* **2008**, *320*, 1326–1329. [[CrossRef](#)]
48. Harrison, J.; Sellars, M.J.; Manson, N.B. Measurement of the optically induced spin polarisation of NV centres in diamond. *Diam. Relat. Mater.* **2006**, *15*, 1326–1329. [[CrossRef](#)]
49. Balasubramanian, G.; Neumann, P.; Twitchen, D.; Markham, M.; Kolesov, R.; Mizuochi, N.; Isoya, J.; Achard, J.; Beck, J.; Tissler, J.; et al. Ultralong spin coherence time in isotopically engineered diamond. *Nat. Mater.* **2009**, *8*, 383–387. [[CrossRef](#)]



© 2019 by the authors. Licensee MDPI, Basel, Switzerland. This article is an open access article distributed under the terms and conditions of the Creative Commons Attribution (CC BY) license (<http://creativecommons.org/licenses/by/4.0/>).